Ordered Porous Carbon with Tailored Pore Size for Electrochemical Hydrogen Storage Application

Baizeng Fang, Haoshen Zhou, and Itaru Honma*

Nano-Energy Materials Group, Energy Technology Institute, National Institute of Advanced Industrial Science and Technology (AIST), Tsukuba, Ibaraki 305-8568, Japan

Received: October 23, 2005; In Final Form: January 26, 2006

Ordered porous carbon with tailored pore size represents an innovative concept in electrochemical hydrogen storage. This work deals with physical characteristics and electrochemical hydrogen storage behavior of the ordered porous carbons with well-tailored pore size, synthesized by a replica technique using hexagonal mesoporous silica as templates. By using a mixture of two surfactants (HTAB and $C_{16}EO_8$) at different ratios, it is possible to control the wall thickness of silica and, consequently, the pore diameter of carbons within a narrow range of 2.1−2.8 nm. In addition, highly developed ultramicroporosity (pore size smaller than 0.7 nm), which plays a predominant role in hydrogen storage, can be produced in the ordered porous carbons. A discharge capacity of up to 527 mAh/g (corresponding to 1.95 wt % hydrogen storage) has been achieved in 6 M KOH for the ordered porous carbon. Furthermore, the ordered porous carbons also possess excellent capacity retainability after charge−discharge cycles and rate capability.

1. Introduction

Hydrogen, which can be produced from renewable energy resources while burning pollution-free, has emerged as one of the most promising candidates for the replacement of the current carbon-based energy services. An important condition for the wide usage of hydrogen as a future fuel, especially for electric vehicles, is the development of a safe, cheap, and simple storage method. Typical methods of storing hydrogen to date have involved storage of compressed gas, liquefied hydrogen, chemisorption in the form of metal hydrides, or physisorption using high surface adsorbents. Hydrogen can be stored in the form of metal hydrides, but there are still obstacles to overcome. High-capacity metal hydrides, such as magnesium-based alloy[1] and intermetallic compound Li_3Be_2[2] (theoretically ca. 7 wt % and 9 wt % of hydrogen storage capacity, respectively), cannot release hydrogen completely unless they are heated to a moderately high temperature. Some commercialized AB_5 type alloys, such as $LaNi_5$, can release hydrogen at room temperature, but have low gravimetric storage density.[3] In recent years, much attention has been paid to elemental carbon, especially single-walled carbon nanotubes (SWNTs) because of their unique characteristics such as high surface reactivity and strong gas adsorption. Dillon and co-worker first investigated hydrogen adsorption properties of as-prepared soot containing only 0.1−0.2 wt % single-walled carbon nanotubes,[4] from which hydrogen adsorption on the carbon nanotube fraction was estimated for ambient conditions to be between ∼5−10 wt %. However, the content of SWNTs in the soot was so low that a large error might be introduced during the estimation of hydrogen storage capacity of pure SWNT materials. In fact, 5−10 wt % of hydrogen storage capacity has been neither reproduced by a pure SWNT material nor explained by theoretical calculation. Although a relative high hydrogen storage capacity on a massive sample weight basis was reported on SWNTs with a large mean diameter of about 1.85 nm by Liu and co-workers and 4.2 wt % was achieved at room temperature under 10 MPa,[5] it seems that high pressure and/or low temperature are necessary to obtain remarkable results. In comparison with this conventional hydrogen storage (i.e., under relatively high pressure and at relatively low temperature), electrochemical hydrogen storage is a more efficient method for hydrogen storage, by which hydrogen is adsorbed in carbon materials during electrochemical decomposition of an aqueous medium.[6,7] This method has found a wide application in nickel/metal hydride (Ni/MH) accumulators.[8] Although lots of research has been done on electrochemical hydrogen storage with alloy materials such as AB_5 (typically $LaNi_5$, a hydrogen storage capacity of ca. 0.96 wt %)[9,10] or Mg-based alloy (ca. 1.0 wt % hydrogen),[11] relatively low capacity obtained from these materials manifests that further improvement in the electrochemical hydrogen storage capacity is necessary. Recently, lots of research has been conducted on electrochemical hydrogen storage in nanostructured materials, such as MoS_2 nanotube (a hydrogen storage capacity of 0.95 wt %),[12] activated carbon (a hydrogen storage capacity of 1.8 wt %),[13,14] SWNTs (corresponding to 1.84 wt % hydrogen),[15] and ordered mesoporous carbon.[16] Relatively high hydrogen storage capacity obtained from nanostructured carbon materials results from the highly developed microporosity.

Encouraged by the good results from nanostructured carbon materials, especially ordered mesoporous carbon, we synthesized ordered porous carbons with well-tailored pore size using template replica technique and investigated their electrochemical behavior for hydrogen storage. Ordered porous carbons with tailored pore size, having ordered interconnected meso- and micropores for fast transportation of mass and highly developed ultramicropores for efficient adsorption of hydrogen, are expected to have higher hydrogen storage capacity than other nanostructured materials. In fact, since their first synthesis by Ryoo and co-workers in 1999,[17] ordered mesoporous carbons with various pore sizes and nanostructures have found wide potential electrochemical applications as catalyst supporting material,[18,19] electrode materials for electric double layer

* Corresponding author. E-mail: i.homma@aist.go.jp.

10.1021/jp056063r CCC: $33.50
Published on Web 02/17/2006

capacitors,[20−22] and for lithium ion batteries.[23] In these cases, the presence of wider pores, preferably in the mesopore range, would be advantageous. However, for electrochemical hydrogen storage application, in addition to interconnected mesopores as fast mass transportation pathways, highly developed micropores (<2 nm), especially ultramicropores (<0.7 nm), are mandatory for efficient hydrogen storage.[16,24−27] For development of a large amount of ultramicropores in templated carbon, a sucrose aqueous solution should be used as carbon precursor because an additional microporosity is formed due to the elimination of water and to the extensive thermal decomposition of sucrose, and consequently the resulting carbon exhibits a much higher total surface area than the initial template. Generally, ordered porous carbons synthesized using sucrose aqueous solution as carbon precursor have relatively large mesopores (>2.7 nm)[16] and relatively low microporosity, resulting from relatively thick pore wall of silica templates (SBA-15, MCM-48). Recently, Lee et al.[28] reported that, by using a mixture of two surfactants (HTAB and $C_{16}EO_8$) at different ratios, it is possible to vary the wall thickness of silica and, consequently, the pore diameter of templated carbons within a narrow range of 2.2−3.3 nm. In this study, we synthesized ordered porous carbons with well-tailored pore size (2.1−2.8 nm) and highly developed ultramicropores using a similar method described by Lee and investigated their physiochemical characteristic and electrochemical hydrogen storage behavior.

2. Experimental Section

Synthesis of the ordered hexagonal mesoporous silica was performed with an aqueous solution of sodium silicate under acidic conditions, which is similar to the procedure described by Lee et al.,[28] except that a higher ratio of HTAB (hexadecyltrimethylammonium bromide) to $C_{16}EO_8$ was set in our study to produce silica with relatively small unit cell size and thin wall thickness suitable for replication of porous carbon with relatively small mesopores (close to 2 nm), together with highly developed microporosity for electrochemical hydrogen storage.

Typically, an aqueous solution of sodium silicate with Na/Si = 0.5 (5.0 wt % SiO_2, 1.3 wt % Na_2O, 93.7 wt % H_2O) was prepared by dissolving colloidal silica (40 wt % SiO_2) in NaOH solution. Two polyoxyethylene hexadecyl ether-type surfactants, $C_{16}H_{33}(C_2H_5O)_2OH$ ($C_{16}EO_2$) and $C_{16}H_{33}(C_2H_5O)_{10}OH$ ($C_{16}EO_{10}$), were mixed in HCl solution (37 wt %) to give nominally $C_{16}EO_8$. Both the silicate (100 mL) and the surfactant (100 mL) solutions were preheated to 308 K. The solutions were combined quickly, shaken vigorously for 2 min, and then agitated for 30 min at 308 K. The mixture was maintained at 308 K for 12 h under static conditions and then heated to 373 K for 12 h. The product was filtered by suction, washed with hot deionized water, slurried in an ethanol−HCl mixture for 30 min, filtered off, and then washed with ethanol. The filtered product was dried at 383 K for 6 h and then calcined in dry air-flow at 823 K for 6 h. Four products were obtained from the starting mole ratios of HTAB, $C_{16}EO_8$:SiO_2:H_2O:HCl = 4:0:16.3:2528:240, 3:1:19.1:3037:215, 2:2:26.5:4267:121, and 1:3:27:4428:96, respectively.

The synthesis of carbons was carried out using the above silica products. Sucrose was used as a carbon source, similar to our previous work on the synthesis of CMK-3 carbon using SBA-15 silica as template,[23] except for the carbonization condition and silica removal method. In a typical synthesis batch, 1.0 g of silica was well mixed with an aqueous solution consisting of 1.25 g of sucrose, 0.14 g of H_2SO_4, and 5.0 g of H_2O. The resultant mixture was dried at 373 K for 6 h and then at 433 K for 6 h. The mixture was impregnated again with an additional amount of sucrose solution consisting of 0.8 g of sucrose, 0.09 g of H_2SO_4, and 5.0 g of H_2O. After being dried at 433 K for 12 h, the sample was heated to 1173 K at a heating rate of 1.6 °C/min under vacuum and held for 4 h. The resultant silica templated carbon was boiled in 1 M NaOH solution (an EtOH−H_2O mixture of 1:1 in volume) twice with magnetic stirring to remove the silica template completely.

Silica and templated carbons were characterized by XRD analysis and BET surface measurement. XRD patterns were recorded with a MacScience-M03XHF22 using Cu K_α irradiation. BET surface measurement was conducted at 77 K with BELSORP by using nitrogen as adsorbent. Pore size distribution was calculated from the adsorption branch of the nitrogen isotherm by the BJH (Barrett−Joyner−Halenda) method. Ordered porous carbons were also characterized by CO_2 adsorption at 273 K.

For electrochemical measurements, a three-electrode cell was constructed, in which porous carbon electrode was used as the working electrode, $Ni(OH)_2$/NiOOH as the counter electrode, saturated calomel (SCE) as the reference electrode, and 6 M KOH as electrolyte. The galvanostatic charge−discharge was conducted in a potential cutoff range from −1.5 to −0.55 V (vs SCE). There was 1 h rest between charge and discharge. The working electrodes for galvanostatic charge−discharge were typically fabricated by pressing the mixture of 95 mg of carbon and 5 mg of poly(tetrafluroethylene) on a nickel mesh. For cyclic voltammetric measurement, the mass of the active material (carbon) in the working electrode is 6.5 mg. Blank experiments (without carbon) have been conducted in galvanostatic and voltammetric techiques for nickel electrode mesh, and also for other collectors, such as Cu mesh, to prove that there is no effect from nickel mesh. The carbon materials were heated at 150 °C for 1 h in a vacuum prior to fabrication of the electrodes.

3. Results and Discussion

3.1. Characterization of Ordered Porous Carbons. The silica synthesized at various surfactant ratios (HTAB:$C_{16}EO_8$) and silica-templated carbons were characterized by X-ray diffraction (XRD) measurements. Figure 1a shows typical powder XRD patterns for the silica (4:0) synthesized using HTAB:$C_{16}EO_8$ = 4:0 after calcination and for the carbon (4:0) after removal of the silica (4:0) template.

The silica (4:0) synthesized exhibits a XRD pattern with a very intense diffraction peak (100) and two weak peaks (110, 200), which are characteristic of a two-dimensional hexagonal structure.[29−31] The carbon (4:0) synthesized also has hexagonal ordered structure, which corresponds to the negative replication of silica (4:0) template. Thermogravimetric analysis (TGA) under an oxygen atmosphere revealed that the maximum silica residue is 2.9 wt % (approximately 0.6 mol %), confirming that the intense XRD peak does not result from the silica template. However, it is noteworthy that only one reflection peak (100) was observed for the carbon (4:0), and the intensity is relatively weak in comparison with silica (4:0), which indicates that carbon (4:0) does not have highly ordered structure. On the other hand, it is found from Figure 1b that with the increasing content of $C_{16}EO_8$ in the mixture of surfactants, the XRD signal intensity of the carbon replicas becomes stronger, even than that of its parent silica template. Strong reflection peaks appear not only at the reflection 100, but also at 110 and 200, which indicates that the porous carbons are highly ordered in these cases. Why does carbon (4:0) have relatively poor structural periodicity? This is due to that the silica (4:0) has the smallest pore diameter

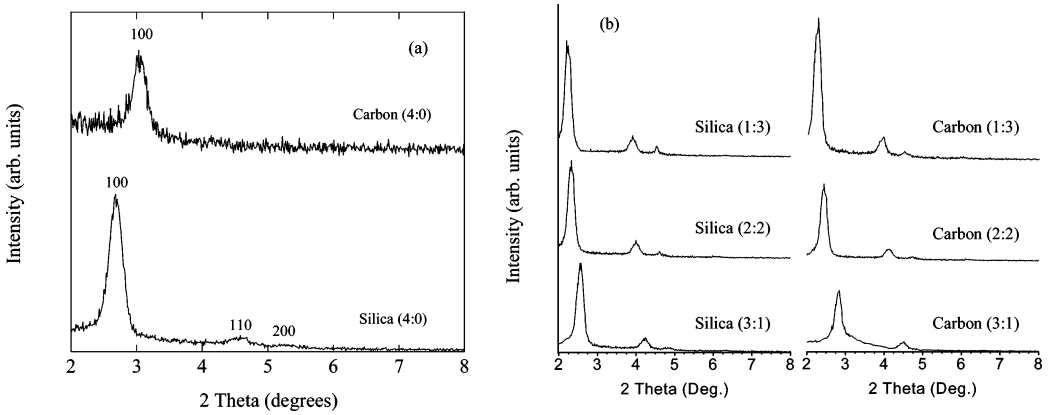

Figure 1. XRD patterns for the silica samples after calcination and for the carbons after removal of the silica templates.

TABLE 1: Structural Properties of Synthesized Silica and Silica-Templated Carbon Obtained at Various Ratios of HTAB to $C_{16}EO_8$

HTAB:$C_{16}EO_8$	silica pore diameter (nm)	silica wall thickness (nm)	carbon pore diameter (nm)
4:0	2.6	1.4	2.1
3:1	2.7	1.5	2.5
2:2	2.9	1.7	2.7
1:3	3.1	1.8	2.8

among all of the silica samples synthesized. It is well known that synthesis of porous carbon with structural periodicity becomes increasingly difficult as the pore diameter of the silica template decreases. This is because larger amounts of organic carbon source per surface area of the pore wall can be infiltrated into mesopores with relatively large pore diameter than into micropores. The carbonization in mesopores with relatively large pore diameter leads to a thick carbon coat that can remain stable and undergo no structural transformation upon the removal of the silica wall.

Table 1 summarizes the structural properties of ordered mesoporous silica and porous carbons characterized by XRD and by N_2 adsorption at 77 K (N_2 adsorption−desorption isotherms and pore size distributions for all of the silica templates and carbon replicas are provided in the Supporting Information).

As shown in Table 1, the carbons exhibit various pore diameters, depending on silica templates with various wall thickness, which increases with the decreasing ratio of HTAB: $C_{16}EO_8$. This tendency was also observed by Lee and co-workers.[28] It is also found that the thickness of the silica walls is not more close to carbon pore diameters. This is because the synthesis of carbon did not follow a simple replication process for the structure of the mesoporous silica. The difference between the silica wall thickness and carbon pore diameter suggests that the structural transformation of the carbon frameworks took place upon the removal of the silica wall. The cause of the structural transformation might be attributed to strain in the carbon frameworks. A large contraction of volume might well occur if pyrolysis of organic compounds to carbon took place without the external constraints. Because silica frameworks in the silica channels prevented this kind of volume contraction, the resultant carbon frameworks could be physically "frustrated". When the silica framework was removed, the structural transformation might take place to relieve the "frustration" or strain. The strain-caused transformation was reasonable, similar to the mesophase transition to relieve the "frustration" in surfactant micelles in the liquid-crystalline state.[32] The increase in wall thickness was reasonable because the amount of silica species interacting with the headgroup corona[33] through hydrogen bonding[34] would increase with the increasing EO segments per surfactant. In addition to the silica wall change, there was also an increase in the silica pore diameter due to the increasing EO content of the surfactants. These simultaneous changes indicate that the EO groups contribute in part to the formation of the silica walls and to the silica mesopores.[28] From Table 1, it is clear that the thickness of mesoporous silica pore and wall can be controlled systematically by the number of the functional groups that can attract silica species such as the ethylene oxide portion of the surfactant. The silica products with various pore diameter and wall thicknesses are suitable as templates for mesoporous carbons with controlled pore diameters.

The porous carbon materials were further characterized by CO_2 adsorption at 273 K to investigate their ultramicroporosity. N_2 adsorption at 77 K is widely used because it covers a large relative pressure range, resulting in adsorption in the whole range of pores. Nevertheless, diffusive problems of the molecules inside the narrow pores at 77 K limit the relevance of this method for the characterization of microporous solids. The usefulness of CO_2 adsorption at 273 K for the micropores characterization of activated carbons is now well established.[35] Although the critical dimension of the CO_2 molecule is similar to that of N_2, the higher adsorption temperature used results in a better diffusion of CO_2 in the narrowest micropores (i.e., pores smaller than 0.7 nm). N_2 adsorption isotherms will be used for determining the total volume of micropores (i.e., pore size smaller than 2 nm), whereas the adsorption of CO_2 at 273 K allows us to assess the narrowest micropores (i.e., pores size smaller than 0.7 nm). The micropore volumes have been calculated from the application of the Dubinin−Radushkevich (DR) equation[36] to the N_2 adsorption at $P/P_0 \leq 0.1$ and the CO_2 adsorption at low relative pressure ($P/P_0 < 0.03$). CO_2 adsorption at 273 K at subatmospheric pressures (i.e., corresponding to relative pressure $P/P_0 < 0.04$) accounts for the narrowest micropores (i.e., ultramicropores with pore size < 0.7 nm).[35] Only at high pressures (i.e., corresponding to relative pressure $P/P_0 > 0.04$), does adsorption of CO_2 in supermicropores (pore size 0.7−2 nm) occur. Therefore, the micropore volume calculated from the application of the DR equation to the CO_2 adsorption at low relative pressure ($P/P_0 < 0.03$) is predominantly attributable to the contribution of ultramicropores. The volumes calculated from the N_2 adsorption and the CO_2 adsorption are noted as $V(N_2)$ and $V(CO_2)$, respectively, in Table 2, where ordered porous carbons are denoted as the $C_{x:y}$ (x:y means the molar ratio of HTAB to $C_{16}EO_8$ for the synthesis of the silica templates).

TABLE 2: Characteristics of the Ordered Porous Carbons Synthesized Using the Silica Templates Obtained at Various Ratios of HTAB to $C_{16}EO_8$[a]

materials	pore size (nm)	area (m^2/g)	$V(N_2)$ (cm^3/g)	$V(CO_2)$ (cm^3/g)	hydrogen stored (mAh/g)
$C_{4:0}$	2.1	1883	0.62	0.51	527
$C_{3:1}$	2.5	1357	0.57	0.44	456
$C_{2:2}$	2.7	1230	0.55	0.41	422
$C_{1:3}$	2.8	1052	0.53	0.38	394

[a] Surface area was calculated by BET method from N_2 adsorption.

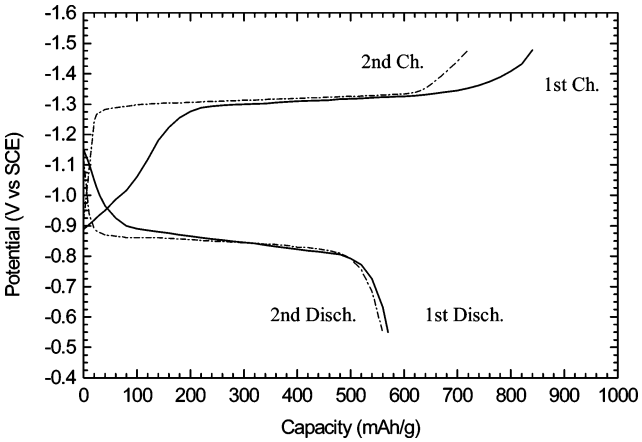

Figure 2. Galvanostatic charge−discharge behavior at 25 mA/g for the carbon (4:0) electrode in 6 M KOH.

Ordered porous carbon materials with high specific surface area are obtained, which can be expected when sucrose is used as carbon precursor. The porous carbons are composed of ultramicropores ($D < 0.7$ nm), supermicropores ($0.7 < D < 2$ nm), and mesopores ($2 < D < 50$ nm). $V(CO_2)$ is lower than $V(N_2)$, confirming the presence of supermicropores in all of the ordered porous carbon. The material $C_{4:0}$ contains the highest amount of ultramicropores (as evidenced by $V(CO_2)$), which is supposed to be highly efficient for hydrogen adsorption.

3.2. Electrochemical Hydrogen Storage in Ordered Porous Carbons. Electrochemical hydrogen storage behavior of the ordered porous carbons was investigated by the galvanostatic charge−discharge technique. Figure 2 shows the first two galvanostatic charge−discharge cycles at 25 mA/g for the ordered carbon (4:0) electrode in 6 M KOH in a potential cutoff range from −1.5 to −0.55 V (vs SCE), where the time axis was converted to the charge−discharge capacity.

For the first charge−discharge cycle, the plateau of the charge curve was observed around −1.28 V (vs SCE), which corresponds to electrochemical reduction of H_2O to H atom (equilibrium potential in 6 M KOH is −0.872 V vs NHE, i.e., −1.14 V vs SCE) and adsorption of H atom in the porous carbon. The plateau of the discharge curve was observed around −0.85 V (vs SCE), and a total discharge capacity of ca. 568 mAh/g was achieved. This discharge capacity cannot be completely attributable to the oxidation of adsorbed hydrogen because ordered porous carbons are excellent candidates for EDLC (electric double layer capacitors) electrodes and can accumulate some charge in the electric double layer. The contribution from the EDL, which was evaluated as 41 mAh/g (assuming a voltage range of 0.6 V for the discharge process) from the cyclic voltammetry measurement (data shown in the Supporting Information), should be subtracted from the total discharge capacity. Thus, a hydrogen desorption capacity of 527 mAh/g is achieved for the ordered porous carbon ($C_{4:0}$) (corresponding to a hydrogen storage capacity of 1.95 wt %). During the first charging process, it was found that there is relatively large charge consumption before water decomposition (around 130 mAh/g provided the water decomposition started when the applied potential is more negative than its equilibrium potential in 6 M KOH), which is greater than the EDL contribution (ca. 40 mAh/g) evaluated from CV measurement. Therefore, other contributions to the charging capacity should be considered, which probably include the effects from reduction of oxygenated surface groups of carbon and/or the impurities in the carbon produced. Oxygen was up to 3.25% (in molar ratio) in the carbon according to elemental analysis, and, during the charging process, reduction of the oxygenated surface groups would take place in the carbon electrode as a side reaction. No such contribution was detected and more well-defined (flat) plateaus for the following charge−discharge cycles were observed, which indicate that the side effects from reduction of oxygenated surface groups and/or the impurities have been eliminated.

The hydrogen storage capacity measured for the other porous carbon materials is listed in Table 2.

It is clear from Figure 3a that the hydrogen storage capacity increases with the total specific surface area, but no straightforward correlation exists between the hydrogen storage capacity and the total specific surface area. No close correlation exists between the hydrogen stored capacity and the micropore volume determined by N_2 adsorption at 77 K (as shown in Figure 3b), which is in agreement with the results reported by Ströbel on disordered carbon materials.[37] On the contrary, an obvious linear relation is observed between the hydrogen storage capacity and $V(CO_2)$ as shown in Figure 3b, which is in agreement with the result reported by C. Vix-Guterl et al. on ordered mesoporous

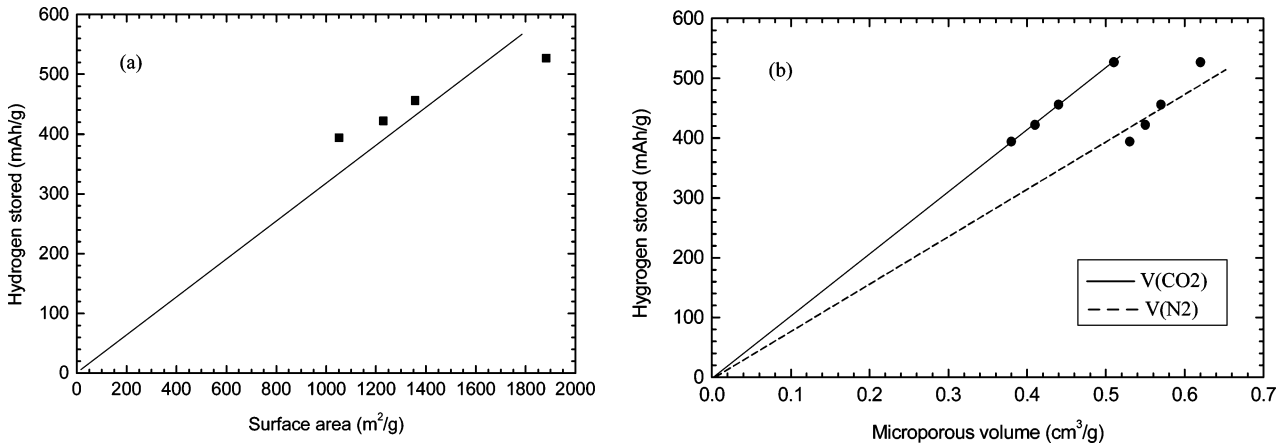

Figure 3. Hydrogen storage capacity of the porous carbons shown against the BET surface area (a) and microporous volume (b) determined by N_2 adsorption at 77 K or CO_2 at 273 K.

TABLE 3: Characteristics and Electrochemical Hydrogen Storage Capacity at a Discharge Rate of 25 mA/g for Various Nanostructured Carbon Materials

material	$V(CO_2)$ (cm^3/g)	hydrogen stored (mAh/g)
carbon (4:0)	0.51	527
activated carbon[a]	0.36	350
SWNT[b]	n.d.[e]	503
MWNT[c]	n.d.	191
ordered carbon[d]	0.34	388

[a] Reference 14. [b] Reference 15. [c] Reference 38. [d] Reference 16. [e] n.d., not determined.

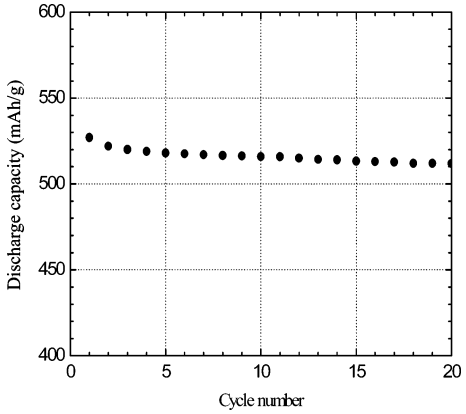

Figure 4. Cycle life performance of the ordered porous carbon ($C_{4:0}$) electrode.

carbons,[16] suggesting that hydrogen adsorption is strongly related to the presence of ultramicropores ($D < 0.7$ nm). Because CO_2 adsorption at 273 K is sensitive to the narrowest micropores, the linear relation observed between the hydrogen storage capacity and the $V(CO_2)$ suggests at least the following two points: (i) a well-developed microporosity associated with a high CO_2 micropore volume is needed to have a high H_2 storage capacity, and (ii) the narrowest micropores seem to be the key factor governing the hydrogen storage capacity of nanostructured carbons.

To further understand the electrochemical hydrogen storage behavior of nanostructured carbon materials, some typical porous carbon materials investigated for this application are collected, and their physical characteristic and electrochemical hydrogen storage capacity are summarized in Table 3.

Although a relatively high hydrogen storage capacity was claimed by Dai[15] for purified SWNTs, no systematic relationship was reported between the indicated purity and the maximum discharge capacity. This suggests that single-walled carbon nanotubes are surely not responsible for the values of sorption observed. Indeed, whatever the method of preparation, nanotubes always contain other forms of carbon, mainly strongly disordered. Therefore, further investigation on the hydrogen storage mechanism of purified SWNTs is necessary. In contrast, high hydrogen storage capacity in the activated carbon,[14] ordered mesoporous carbon,[16] and carbon (4:0) has been proved to be predominantly attributable to the highly developed ultramicroporosity in these materials. In comparison with the activated carbon, more ultramicroporosity has been developed in the carbon (4:0), resulting in a higher hydrogen storage capacity in the latter. In addition, ordered nanostructure provides additional advantages over disordered nanostructured carbons such as activated carbons, providing not only rapid transport of H_2O molecules to the active sites where electrochemical reduction of H_2O takes place, resulting in fast hydrogen production kinetics, but also facilitating fast transfer (diffusion) and adsorption (or desorption) of hydrogen atoms, and accordingly contributing to some extent to the improved capacity.

For a rechargeable electrode material, an important requirement is the capacity retainability after certain charge−discharge cycles. Figure 4 shows the cycling characteristics of the ordered porous carbon ($C_{4:0}$) electrode. It is clear that after 20 cycles of charge−discharge the capacity loss is less than 2.8%, indicating excellent capacity retainability for the ordered porous carbon electrode.

After 20 charge−discharge cycles, the discharge curves and discharge capacity of the porous carbon ($C_{4:0}$) electrode were evaluated at various charge−discharge rates and shown in Figure 5. As seen in Figure 5a, a larger polarization was observed at 3000 mA/g than that at 25 mA/g, which is primarily attributable to a larger ohmic drop. A well-defined discharge plateau is still available and indicates that the effect from mass diffusion is relatively small in comparison with the contribution from ohmic drop. At a low discharge rate, hydrogen storage capacity can be calculated simply from the difference between the total discharge capacity and EDL contribution. However, it becomes difficult to determine EDL contribution from CV measurement at a high scan rate. Despite this, the hydrogen storage capacity at high discharge rate (i.e., 3000 mA/g) can be roughly estimated according to the length of the well-defined discharge plateau.

Figure 5b shows the discharge capacities (hydrogen storage capacity) obtained at various discharge rates after 20 charge−discharge cycles. Although the discharge capacity decreases with the increasing discharging rates, the hydrogen storage capacity still remains at a high level (343 mAh/g) even at a very high

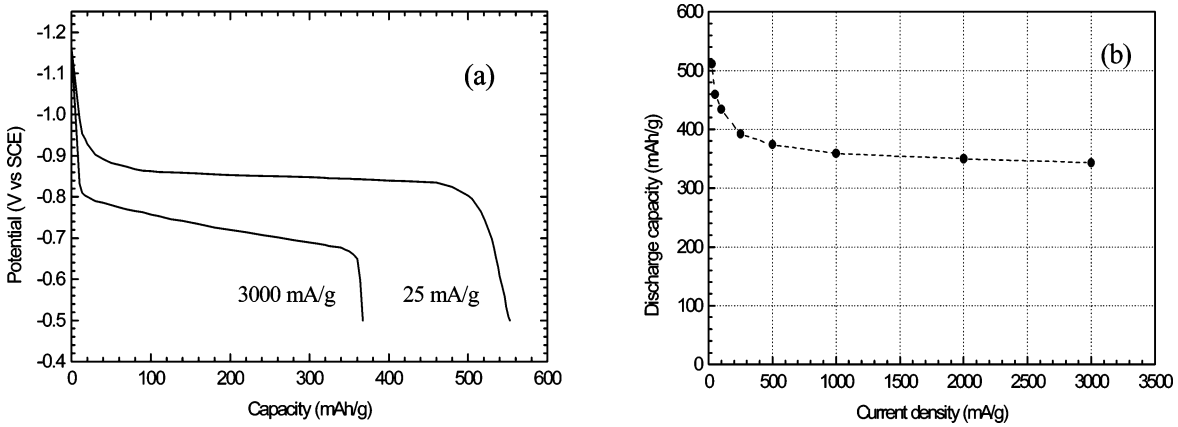

Figure 5. Discharge curves (a) and discharge capacity (hydrogen storage capacity) (b) of the porous carbon (4:0) electrode obtained at various rates after 20 cycles.

discharge rate (i.e., 3000 mA/g), indicating that carbon material possesses excellent rate capability and can deliver the adsorbed hydrogen very quickly at high discharge rates. A high capacity available at high discharge rates reflects the dominance of regular interconnected mesopores among electrochemically usable pores. Interestingly, activated carbon was reported to have a relatively high capacity of electrochemical hydrogen storage, that is, 350 mAh/g at a discharge rate of 25 mA/g,[14] mainly resulting from its developed extramicroporosity. However, unlike the ordered porous carbon, activated carbon could only deliver hydrogen stored at a relatively low discharge rate (typically less than 100 mA/g). At a high discharge rate (i.e., greater than 1000 mA/g), discharge capacity of activated carbon is fairly small, which is mainly attributable to the disordered structure of the activated carbon that is unfavorable for fast mass transportation (H_2O and H).

4. Conclusions

Ordered porous carbons with well-tailored pore size can be synthesized by the control of pore and wall thickness of the silica templates, which can be realized by varying the ratio of surfactants HTAB to $C_{16}EO_8$. Highly developed microporosity can be produced in the porous carbons with tailored pore size (within a narrow range 2.1−2.8 nm). Highly developed ultramicroporosity (pore size smaller than 0.7 nm), playing a predominant role in hydrogen storage, and ordered interconnected meso- and micropores, serving as rapid mass transportation pathway, provide ordered porous carbons with very high hydrogen storage capacity. A hydrogen storage capacity up to 527 mAh/g was achieved for the porous carbon (4:0) with well-tailored pore distribution, which is much higher than those obtained from other nanostructured carbon materials and from the most popular electrode material $LaNi_5$ alloy for electrochemical hydrogen storage. Furthermore, the porous carbon synthesized also possesses excellent cycling capacity retainability and high-rate capability and is an efficient and promising electrode material for electrochemical hydrogen storage.

Supporting Information Available: N_2 adsorption isotherms and pore size distribution of silica and templated carbons. Cyclic voltammogram for carbon (4:0) in 6 M KOH. This material is available free of charge via the Internet at http://pubs.acs.org.

References and Notes

(1) Stampfer, J. F., Jr.; Holley, C. E., Jr.; Suttle, J. F. *J. Am. Chem. Soc.* **1960**, *82*, 3504.
(2) Zaluska, A.; Zaluski, L.; Stroem, J. O. *Appl. Phys.* **2001**, *A72*, 157.
(3) Cohen, R. L.; Wernick, J. H. *Science* **1981**, *214*, 108.
(4) Dillon, A. C.; Jones, K. M.; Bekkedahl, T. A.; Kiang, C.; Bethune, D. S.; Heben, M. J. *Nature* **1997**, *386*, 377.
(5) Liu, C.; Fan, Y. Y.; Liu, M.; Cong, H. T.; Cheng, H. M.; Dresselhaus, M. S. *Science* **1999**, *286*, 1127.
(6) Frackowiak, E.; Béguin, F. *Carbon* **2002**, *40*, 1775.
(7) Jurewicz, K.; Frackowiak, E.; Béguin, F. *Electrochem. Solid-State Lett.* **2001**, *4*, A27.
(8) Sakai, T.; Uehera, I.; Ishikawa, H. *J. Alloys Compd.* **1999**, *762*, 293.
(9) Simicic, M. V.; Zdujic, M.; Jelovac, D. M.; Rakin, P. M. *J. Power Sources* **2001**, *92*, 250.
(10) Jurczyk, M.; Nowak, M.; Jankowska, E.; Jakubowicz, J. *J. Alloys Compd.* **2002**, *339*, 339.
(11) Xue, J.; Li, G.; Hu, Y.; Du, J.; Wang, C.; Hu, G. *J. Alloys Compd.* **2000**, *307*, 240.
(12) Chen, J.; Kuriyama, N.; Yuan, H.-T.; Takeshita, H. T.; Sakai, T. *J. Am. Chem. Soc.* **2001**, *123*, 11813.
(13) Jurewicz, K.; Frackowiak, E.; Béguin, F. *Fuel Process. Technol.* **2002**, *77*−*78*, 415.
(14) Jurewicz, K.; Frackowiak, E.; Béguin, F. *Appl. Phys. A* **2004**, *78*, 981.
(15) Dai, G.-P.; Liu, C.; Liu, M.; Wang, M.-Z.; Cheng, H.-M. *Nano Lett.* **2002**, *5*, 503.
(16) Vix-Guterl, C.; Frackowiak, E.; Jurewicz, K.; Friebe, M.; Parmentier, J.; Béguin, F. *Carbon* **2005**, *43*, 1293.
(17) Ryoo, R.; Joo, S. H.; Jun, S. *J. Phys. Chem. B* **1999**, *103*, 7743.
(18) Yu, J.-S.; Kang, S.; Yoon, S.-B.; Chai, G. *J. Am. Chem. Soc.* **2002**, *124*, 9382.
(19) Joo, S. H.; Choi, S. J.; Oh, I.; Kwak, J.; Liu, Z.; Terasaki, O.; Ryoo, R. *Nature* **2001**, *412*, 169.
(20) Lee, J.; Yoon, S.; Oh, S. M.; Shin, C.-H.; Hyeon, T. *Adv. Mater.* **2000**, *12*, 359.
(21) Lee, J.; Yoon, S.; Hyeon, T.; Seung, M. O.; Kim, K. B. *Chem. Commun.* **1999**, 2177.
(22) Zhou, H.-S.; Zhu, S.; Hibino, M.; Honma, I. *J. Power Sources* **2003**, *122*, 219.
(23) Zhou, H.-S.; Zhu, S.; Hibino, M.; Honma, I.; Ichihara, M. *Adv. Mater.* **2003**, *15*, 2107.
(24) Foley, H. C. *J. Microporous Mater.* **1995**, *4*, 407.
(25) De la Casa-Lillo, M. A.; Lamari-Darkrim, F.; Cazorla-Amoros, D.; Linares-Solano, A. *J. Phys. Chem. B* **2002**, *106*, 10930.
(26) Rzepka, M.; Lamp, P.; De la Casa-Lillo, M. A. *J. Phys. Chem. B* **1998**, *102*, 10894.
(27) Texier-Mandoki, N.; Dentzer, J.; Piquero, T.; Saadallah, S.; David, P.; Vix-Guterl, C. *Carbon* **2004**, *42*, 2744.
(28) Lee, J.-S.; Joo, S.-H.; Ryoo, R. *J. Am. Chem. Soc.* **2002**, *124*, 1156.
(29) Hou, Q.; Margolese, D. I.; Ciesla, U.; Feng, P.; Gier, T. E.; Sieger, P.; Leon, R.; Petroff, P. M.; Schüth, F.; Stucky, G. D. *Nature* **1994**, *368*, 317.
(30) Attard, G.; Glyde, J. C.; Göltner, C. G. *Nature* **1995**, *378*, 366.
(31) Zhao, D.; Feng, J.; Huo, Q.; Melosh, N.; Fredrickson, G. H.; Chmelka, B. F.; Stucky, G. D. *Science* **1998**, *279*, 548.
(32) Impéror-Clerc, M.; Davidson, P.; Davidson, A. *J. Am. Chem. Soc.* **2000**, *122*, 11925.
(33) Seddon, J. M.; Templer, R. H. *Philos. Trans. R. Soc. London, Ser. A* **1993**, *344*, 377.
(34) Huo, Q.; Margolese, D. I.; Ciesla, U.; Demuth, D. G.; Feng, P.; Gier, T. E.; Sieger, P.; Chmelka, B. F.; Schüth, F.; Stucky, G. D. *Nature* **1994**, *368*, 317.
(35) Cazorla-Amoros, D.; Alcaniz-Monge, J.; De la Casa-Lillo, M. A.; Linares-Solano, A. *Langmuir* **1998**, *14*, 4589.
(36) Dubinin, M. M. In *Chemistry and Physics of Carbon*; Walker, P. L., Jr., Ed.; Marcel Dekker: New York, 1966; Vol. 2, p 51.
(37) Ströbel, R.; Jörissen, L.; Schliermann, T.; Trapp, V.; Schültz, W.; Bohmhammel, K. *J. Power Sources* **1999**, *84*, 221.
(38) Qin, X.; Gao, X.-P.; Liu, H.; Yuan, H.-T.; Yan, D.-Y.; Gong, W.-L.; Song, D.-Y. *Electrochem. Solid-State Lett.* **2000**, *3*, 532.